

Progress of 2D Semiconductor-based photocatalysts

Subjects: [Chemistry, Physical](#) | [Physics, Applied](#) | [Nanoscience & Nanotechnology](#)

Contributor: Xiaoyong Yang , Deobrat Singh , Rajeev Ahuja

A complete view of basic principles and mechanisms with regard to improving the structure stability, physical and chemical properties of the low dimensional semiconductor-based photocatalysts is presented here. Various 2D semiconductor-based photocatalysts show a high electrochemical property and photocatalytic performance due to their ultrathin character, high specific surface area with more activity sites, tunable bandgap to absorb sunlight and versatile options in structural assembly with other nanosheets. At present, most photocatalysts still need rare or expensive noble metals to improve the photocatalytic activity, which inhibits their commercial-scale application extremely. Thus, developing less costly, earth-abundant semiconductor-based photocatalysts with the efficient conversion of sunlight energy remains the primary challenge. A concise overview of different types of 2D semiconductor-mediated photocatalysts is given to figure out the advantages and disadvantages for mentioned semiconductor-based photocatalysis, including the structural property and stability, synthesise method, electrochemical property, and optical properties for H₂/O₂ production half-reaction along with overall water splitting.

Ultrathin semiconductor-based photocatalysts

Hydrogen evolution reaction

Oxygen evolution reaction

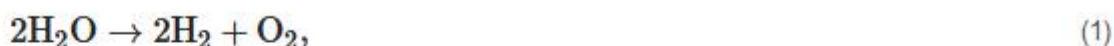
Overall water splitting

1. Introduction

Nowadays, the biggest technological challenges for human beings are the increasing consumption of resources and energy and the related environmental pollution problem all over the world. For example, the worldwide energy consumption will expect to reach up to 815 quadrillion Btu in 2040 due to the growing global production and population [\[1\]\[2\]](#). However, the huge energy resources in the earth mainly originate from non-renewable coal, oil, natural gas, and nuclear energy, and their reserves are limited. Although the energy is released by combustion on the application of these fossil fuels, a series of critical environmental problems—water contamination, greenhouse gas emissions, global warming, and the emergence of a hole in the ozone layer—occur at the same time. Thus, lots of scientists, politicians, industry groups are encouraged to seek new and sustainable alternative energy resources. Every day the sun radiates an enormous amount of energy for our planet, which has attracted great attention as a promising alternative energy source for cutting greenhouse gas emissions and providing the current and future human energy demand. However, it is not nearly sufficient, therefore, the harvest and conversion of solar energy into other kinds of energy is a priority to resolve [\[3\]\[4\]\[5\]](#). At present, photovoltaic cells are already a popular sight on rooftops to directly convert solar energy into electricity. However, electricity presents its own

challenges in that it would have to be used immediately or be stored in a secondary device at a high energy density, such as capacitors or batteries. In comparison with converting solar energy into electricity, synthesizing storable, transportable chemical fuels via photocatalytic processes would be a more attractive approach, in which the harnessing of energy in sunlight would be stored in the form of molecular bonds through a thermodynamic "uphill reaction" (see Equation (1)). Up to now, a photocatalysis technique has been used in different application fields, such as water splitting to produce hydrogen [6][7], sterilization [8], wastewater treatment and self-cleaning materials [9], decomposition of crude spills [10][11], dye-sensitized solar cell and inactivation of cancer cells [12][13].

Hydrogen (H₂) is a clean and carbon-free fuel with high specific enthalpy. Whereas, until now, around 95% of the world's hydrogen fuel is mainly sourced from natural gas, by reacting methane with steam using fossil fuel to produce hydrogen and carbon dioxide (CO₂). Thus the production of hydrogen from methane is a kind of fossil fuel product rather than renewable energy. The critical method to utilize hydrogen production is developing an effective H₂-preparation approach without ever seeing fossil fuels. The method using photocatalytic materials to produce hydrogen has been demonstrated since 1972 according to the following reaction equation,



$$\Delta E^0 = 1.23 \text{ eV}, \Delta G^0 = +237.2 \text{ kJ mol}^{-1},$$

This photocatalytic process is driven by a thermodynamic "uphill reaction" of solar energy with a large change of $\Delta G^0 = 1.23 \text{ eV}$ (237.13 kJ mol⁻¹) per photon [14]. Here, the photocatalytic materials require four-electron generations according to Equation (2) to endure this reaction of water,



$$\text{NHE, pH} = 0, \text{ vs. } \Delta E^0 = 237.13 \text{ kJ mol}^{-1}$$



$$\text{NHE, pH} = 0, \text{ vs. } \Delta E^0 = 0 \text{ kJ mol}^{-1}$$

Therefore, the surface of the photocatalytic materials should be struck using suitable energy with the corresponding photons. The estimated solar photon flux density (Q) is 2000 μmol s⁻¹m⁻² [15]. While the previous reports found the holes took less than 2 μs to react with the water vapor while the oxygen took 10–100 μs to capture the electrons in P25 TiO₂ [15][16], thus, gaining the solar photon flux of photocatalytic materials is a big challenge. Since Honda and Fujishima firstly discovered the Pt/TiO₂ electrode could be used to complete the water-

splitting reaction to generate H₂, utilizing artificial photosynthesis producing solar hydrogen production has become a promising strategy for converting and storing solar energy into chemical H₂ fuel [17]. To date, numerous efforts have been devoted to realizing photocatalytic H₂ production from water, including semiconductor-based heterogeneous systems [1][18][19][20][21][22][23][24][25], molecular material-based homogeneous systems [26][27][28][29][30], and organic-inorganic hybrid systems [31][32][33]. Subsequently, the research field is also expanding fast and attracting lots of scientists from chemistry and material science to physics and computational science. For example, chemists devote themselves to developing molecular photosensitizers and catalysts as well as establishing the relationship between the structure of materials and the corresponding property for H₂ production systems [34][35][36][37]. For material scientists, they try their best to design and synthesize new architecture materials with the high photocatalytic performance [38][39][40]. With regard to physicists, they focus themselves on dealing with the fundamental physical mechanisms of semiconductor-based heterogeneous photocatalysts and reduce the recombination of photon-electron pairs as well as their traveling distance [41][42][43]. This natural synergy could help in the development of materials science and generate a big future for renewable energy.

There are three major steps to overall photocatalytic split water for a semiconductor photocatalyst: (1) the absorption of photons on the surface of a semiconductor, with appropriate energy, which can stimulate electron transfer to the conduction band position from the valence band position and generate electron-hole pairs (e^-h^+), (2) the separation and migration of charge carriers on the surface of the material at a short span of time; (3) the impingement between the corresponding free electrons and holes on the surface of the system to complete the water-splitting reaction to generate H₂ or O₂, as depicted in [Figure 1](#). Whereas, the recombination of the free electrons and the excited holes may readily happen in the second step, giving rise to poor photocatalytic activity of the nanocrystal surface. Accordingly, the suitable bandgap and the corresponding levels of the conduction and valence bands could aid the light absorption on the surface of the semiconductor photocatalyst, even at a low solar energy flux density. In general, when semiconductor-based photocatalysts show a more negative level of the bottom of the conduction band than the reduction potential of H⁺/H₂ (0 V vs. NHE, pH = 0) and a more positive level of the top of the valence band than the oxidation potential of O₂/H₂O (1.23 V vs. NHE, pH = 0), the photocatalysis of water is more thermodynamically feasible [44][45]. It should be mentioned that the extreme challenge for the overall process of photocatalytic water splitting is to reduce the recombination of four-electron-four-hole as well as shorten their traveling distance [46][47]. Equations (2) and (3) are the standard half-reactions for H₂ and O₂ evolution, respectively, the corresponding schematic illustration is shown in [Figure 1](#). In addition, one of these half-reactions can be substituted by an appropriate sacrificial reductant in the half-reaction systems. For example, methanol [48], triethylamine [49], ethanol [50], Na₂S/Na₂SO₃ pairs [51] and triethanolamine [52] are the most commonly used sacrificial reductants. In addition, ascorbic/lactic acid [53][54], ethylene diamine tetra-acetic acid [55], and sacrificial oxidant [56] are also reported in the previous work. Over the past four decades, various semiconductor-based photocatalysts have been designed, synthesized, and developed with a broader purpose to obtain a solar energy flux (step 1 in [Figure 1](#)) and efficient reduction of the charge carriers recombination and to shorten the migration for the charge carriers (step 2 in [Figure 1](#)). For example, lots of bandgap engineering methods are applied to improve the sunlight absorption, even at a low flux density, for wide bandgap semiconductors, including ions/defects doping and forming solid solutions [57][58][59], hybridization with small

bandgap semiconductors [60][61], disorder engineering [62], and surface plasmonic enhancement [63]. In addition, different kinds of nanostructured semiconductors have been synthesized to obtain efficient charge separation and transportation, such as nanoparticles, porous nanospheres, nanowires, nanobelts, nanotubes, and nanosheets [64][65]. It is worth mentioning that the formation of a vertical or in-plane hetero-junction using two or more than two semiconductors has been extensively explored to improve the charge carrier's separation and shorten their traveling distance [66][67]. Until now, the first two steps in [Figure 1](#) have made significant advancement in photocatalytic water splitting. The majority of research achievements are only efficient for either proton reduction or water oxidation. The co-photocatalysts, which could work for overall water splitting, have not been overwhelmingly investigated since the combination of a suitable bandgap, an appropriate bottom of the conduction band and an appropriate top of the valence band is difficult to engineer [68]. However, a few materials, such as $\text{Rh}_{2-y}\text{Cr}_y\text{O}_3$ [69] and $\text{Rh-Cr}_2\text{O}_3$ [70][71], are proposed as the most active co-catalysts. However, these noble-metal based co-catalysts can not be used in a large scale energy production because the resources of noble metals are limited. Hence, there is significance in exploring co-catalysts with low cost and high efficiency.

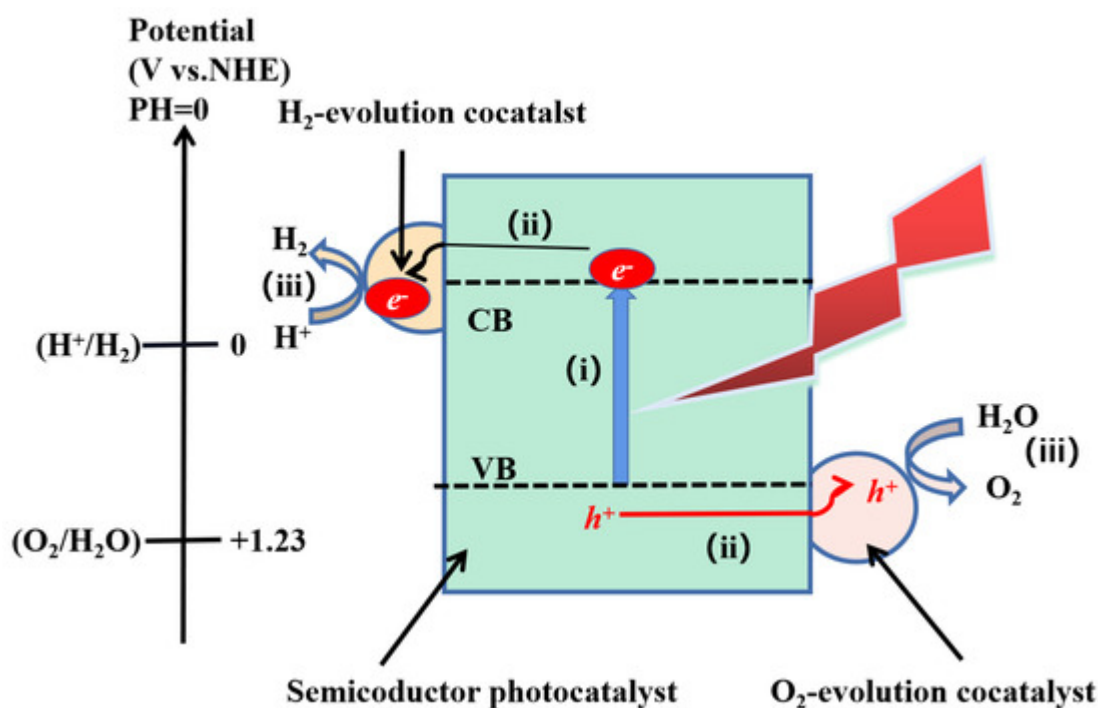


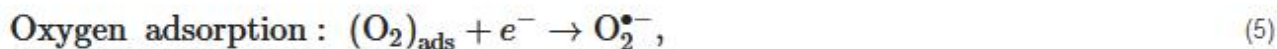
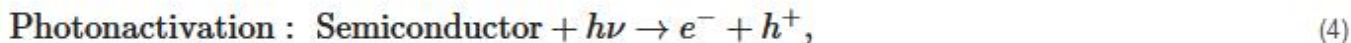
Figure 1. Schematic diagram of the three major steps of overall photocatalytic water splitting on a semiconductor photocatalyst [18].

On the other hand, nanoparticles, porous nanospheres, and nanowires have recently attracted a large amount of attention in the process of water splitting in that they possess unconventional and fancy physical and chemical properties, which may be easier to meet the requirements for overall photocatalytic splitting water compared to their bulk counterparts [30][72][73][74][75][76]. First, these different nanostructures could decrease the rate of charge carriers recombination and let them travel a very small distance, which largely enriches the selectivity of photocatalytic materials and paves a new path to design an effective photocatalysis. Second, 2D nanostructured photocatalysts could have more active sites for electrochemical reactions due to their larger surface areas. Third,

quantum confinement effects in 2D metallic and semiconductor nanostructures dependent on the size and morphology of photocatalysts could open a new approach to engineer the processes of sunlight harvesting. It is because the quantum size effects can restrict electrons in order to accommodate the additional atom, platelike nanoparticles, disk, or cluster, resulting in an increase of energy levels and HOMO-LUMO bandgap. For 1D quantum confined materials, it is found that the modification of the aspect ratio of nanorods could largely tune the optical response properties [77]. Last but not least, various 2D nanomaterials provide more sources to integrate heterogeneous structures with multiple functional properties. On the other hand, for the majority of 3D semiconductors, it is commonly ignored to distinguish the electronic and optical bandgaps due to the small exciton binding energy. While the distinction between electronic and optical bandgaps in 2D nanomaterials is significant and obvious. The Bethe–Salpeter equation is frequently used to predict the exciton binding energy and optical bandgap. Furthermore, most of the 2D materials exhibit more soft elastic constants, which could have extra application compared to bulk 3D counterparts. Particularly, the band edge positions and bandgaps are very sensitive to small strains with a significant extent, thus it could facilitate tuning the photocatalytic performance of 2D nanomaterials as photocatalysts. Herein, the current review work covers the fundamental mechanism of overall photocatalytic water splitting and recent progress in the use of two dimensional (2D) semiconductor-based nanomaterials and their nanoheterostructure composites with a focus on the relationship between the structural property of the nanomaterials and their photocatalytic activity. It begins by introducing the various mechanisms of photoexcited carriers on different 2D semiconductor-based nanomaterials during photocatalytic overall water splitting to provide a whole view for the principle of work on the basis of thermodynamics half-reactions. Then, we compare the general structural property, advantages in electronic and surface properties, and electrochemical performances to pursue high efficiency of water splitting on the different 2D semiconductors, including carbon nitride ($g-C_3N_4$), boron nitride, black phosphorus, transition metal oxides (TMOs), transition metal dichalcogenides (TMDs), MXenes, perovskite nanosheets, nanoheterostructure composites, metal-organic frameworks (MOFs), covalent organic frameworks (COFs). Subsequently, some commonly used synthetic methods for 2D nanomaterials are summarized in section 4. Toward the end, we conclude the current research status with a perspective on the challenges of 2D semiconductor-based photocatalysts for photocatalysis applications.

2. Mechanisms of Overall Photocatalytic Water Splitting

In previous researches, the mechanisms of 2D and 3D materials as photocatalysts to split water have been extensively reported. With regard to semiconductors, the absorbed photon should possess higher energy ($h\nu$) than the corresponding bandgap of the semiconductor in order to excite the electrons to the empty conduction band (CB) position from the filled valence band (VB) position of the semiconductor photocatalyst. Then the excited electrons and holes pair (e^-h^+) is formed according to the following expression,



The bandgap of a single semiconductor photocatalyst should meet the requirements of reduction reaction potential with 0 eV for catalyzing H₂O into H₂ (H⁺/H₂) and oxidation reaction potential with +1.23 eV for oxidizing H₂O into O₂ (O₂/H₂O) in pH = 0 reactant solution at a normal hydrogen electrode (NHE), as shown in [Figure 2a](#). This mechanism is called one-step water splitting. Alternatively, an appropriate water redox shuttle mediator can connect to two different semiconductors or even more to form a hybrid semiconductor. Detailedly, the H⁺/H₂ reduction, and O₂/H₂O oxidation can occur on two separately semiconductors in hybrid materials in order to make the photon-induced e⁻-h⁺ pairs separate and overall water splitting. This system is called the Z-scheme system [\[78\]](#) [\[79\]](#).

In a system with a semiconductor electrode immersing in an electrolyte solution, the electrons transfer take place spontaneously in order to keep the balance between the Fermi level (E_f) of the semiconductor photocatalyst and the redox potential of the electrolyte solution. Specifically, if E_f of the semiconductor photocatalyst is higher than the oxidation potential of the electrolyte solution, then the semiconductor photocatalyst will accept electrons from the electrolyte solution - and the converse is also true. It is known, in a semiconductor, the electrons density is finite but the valence band (VB) and conduction band (CB) positions at the interfaces are regarded as fixed, thus the electron transfer can cause band bending. The space charge layer could induce an intrinsic electric field, which is helpful to separate the charge [\[80\]](#). For example, a n-type semiconductor can work as a photoanode for oxygen evolution, thus photon-generated holes will accumulate on the surface of the semiconductor, whereas the counter electrode will accept the corresponding electrons through an external circuit, as shown in [Figure 2c](#) [\[7\]](#). In this oxidation reaction, the maximum valence band (MVB) of the photon-anode should be lower than the oxygen evolution potential of -5.67 eV by ΔE_V to allow the n-type semiconductor generating oxygen. In contrast, the p-type semiconductors act as photocathodes for reduction reaction to catalyze H₂O into H₂ if the minimum conduction band edge (MCB) is higher than the hydrogen evolution potential of -4.44 eV by , as depicted in [Figure 2d](#). Accordingly, in both cases, the excited carriers by sunlight could drive the photoelectrochemical reactions on photoanodes. While, if E_f of the counter electrode fails the redox reactions, an external voltage can be used to compensate for the potential deficiency. It is worthy to mention that if the kinetic overpotential of ΔE_V or is larger, then the required bias voltage should be larger to make the redox reactions successfully on the counter electrode. In the Z-scheme water splitting system, two different photocatalysts, i.e. photoanode and photocathode,

are combined in tandem. Then the sunlight can be efficiently utilized than that in the one-step water splitting systems since the maximum energy required to drive the photoelectrodes is reduced, as shown in [Figure 2e](#).

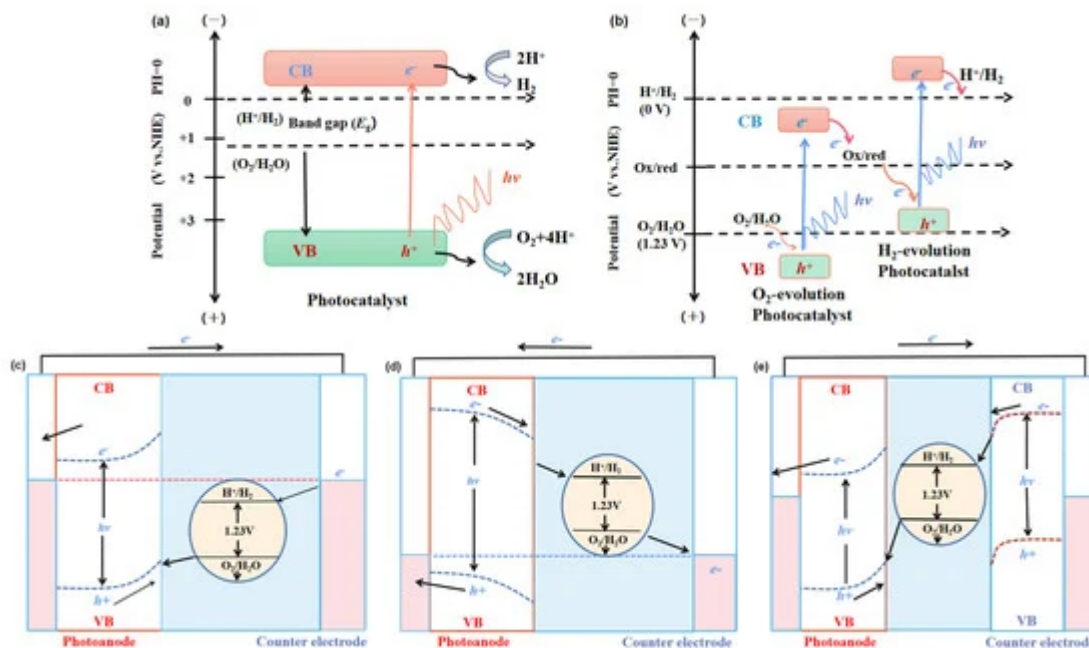


Figure 2. Energy schematic diagram based on (a) one-step water splitting and (b) Z-scheme mechanism; and photoelectrochemical water splitting using (c) a photoanode, (d) photocathode, and (e) photoanode and count electrode in tandem systems for photocatalytic water splitting, respectively [\[81\]](#).

3. Classification of 2D Semiconductors for Photocatalysts

To date, a great amount of 2D nanosheets have been synthesized by various chemical and/or physical methods, which are mainly divided into two types, layered and non-layer structural materials. With regard to layered materials, the in-plane layer is formed by connecting the in-plane atoms by strong chemical bonding. However, the weak van der Waals interaction plays an important role in stacking these monolayers to form bulk crystals [\[82\]](#). The representative layered material is graphite crystal, which is stacked by many graphene layers via weak van der Waals force. In addition, nitrides (such as g-C₃N₄, h-BN, GaN, Ca₂N), black phosphorus (BP), Xenes, transition metal dichalcogenides (TMDs), transition metal oxides are also layered materials, as shown in [Figure 3](#). The exfoliation of highly anisotropic layered materials into a 2D monolayer can use the micro-mechanical cleavage method, mechanical force-assisted liquid exfoliation method, or ion intercalation-assisted liquid exfoliation, which are collectively known as top-down exfoliation methods. It is because highly anisotropic layered materials possess strong in-plane bonds in each layer with high covalent character but weakly stack the monolayers via ionic or Van der Waals interactions [\[82\]](#). In contrast, other solid crystals, generally crystallized into three dimensions (3D) bulk via atomic or chemical bonding, including bulk metals, metal oxide matrices, metal chalcogenide matrices, and polymers, can form 2D inorganic nanosheets by the bottom-up approach, which includes a wet-chemical route and

chemical vapor deposition (CVD) [83][84][85]. Particularly, a variety of solid materials can be formed relying on the coordination mode and arrangement of atoms as well as the stacking orders among every monolayer [86][87][88]. All these factors could have a significant effect on the physical and chemical properties and functionalities of the crystal materials [86][87][88][89][90][91]. The promising ultrathin 2D photocatalysts for photocatalytic water splitting can mainly be categorized into metal-composite oxides, metal hydroxides, TMDs, MXenes, and metal-free photocatalysts, metal-organic frameworks (MOFs), covalent-organic frameworks (COFs), and so on. In this section, the crystal structural information and the photocatalysis properties of these widely explored 2D semiconductor-based photocatalysts will be detailedly introduced based on their composition.

H	Organic materials																He
Li	Be	Transition Metal Dichalcogenides										B	C	N	O	F	Ne
Na	Mg	Graphene and graphene like materials										Al	Si	P	S	Cl	Ar
K	Ca	Sc	Ti	V	Cr	Mn	Fe	Co	Ni	Cu	Zn	Ga	Ge	As	Se	Br	Kr
Rb	Sr	Y	Zr	Nb	Mo	Tc	Ru	Rh	Pd	Ag	Gd	In	Sn	Sb	Te	I	Xe
Cs	Ba	La-Lu	Hf	Ta	W	Re	Os	Ir	Pt	Au	Hg	Tl	Pb	Bi	Po	At	Rn
2D Metal-Composite Oxides	CuO, ZnO, CoO		Fe ₂ O ₃ , Bi ₂ O ₃		BiVO ₄ , CuWO ₄ , CuFeO ₄			Perovskite-type: Bi ₄ Ti ₃ O ₁₂ , Ca ₂ Ta ₂ TiO ₁₀ , LaNb ₂ O ₇ ; and so on			Others						
	MoO ₃ , WO ₃		TiO ₂ , Cu ₂ O		CaFe ₂ O ₄ , ZnFe ₂ O ₄ , CuBi ₂ O ₄												
2D Transition Metal Dichalcogenides	Semiconducting dichalcogenides: MoS ₂ , MoSe ₂ , MoTe ₂ , WS ₂ , WSe ₂ , WTe ₂					Metallic dichalcogenides: NbS ₂ , NbSe ₂ , NbTe ₂ , TaS ₂ , TaSe ₂ , TaTe ₂					Janus Semiconducting dichalcogenides: MoSSe, MoSTe, MoTeSe, WSSe, WSeTe, WSTe						
Metal-free 2D nanosheets	Graphene, <i>g</i> -C ₃ N ₄ , <i>h</i> -BN, <i>h</i> -BCN, Borophene, <i>h</i> -BO					MXenes: Ti ₃ C, Ti ₃ C ₂ , Ti ₃ C ₃ , Zr ₂ C, Ti ₄ N ₃ , Hf ₂ C, V ₂ C, Nb ₂ C, V ₂ N, (Ti _{0.5} V _{0.5}) ₂ C, (Nb _{0.8} Ti _{0.2}) ₄ C ₃ , (Mo _{0.5} Ti _{0.5}) ₄ C ₃ , (Mo _{0.67} Ti _{0.33}) ₃ C ₂											

Figure 3. Periodic table with highlighted elements for typical ultrathin 2D materials.

4. Synthesis Methods for 2D Materials

Various approaches have been explored to synthesize 2D monolayers or few-layer nanosheets and tailor the structure with corresponding physical and chemical properties in order to suit different kinds of applications. Generally, the synthesis methods can be classified into two types based on the composition, crystal phase, and surface property of materials: (1) the top-down method, which mainly depends on the exfoliation of 2D monolayers from their parental layered bulk material by overcoming the weak interlayer binding force; (2) the bottom-up method, which is more versatile in principle than most 2D nanosheets, might be gained by this method. In this section, some representative methods to prepare 2D materials are discussed and summarized.

4.1 Micromechanical cleavage using scotch tape

Micromechanical cleavage using scotch tape is a simple and conventional method to fabricate thin flake by peeling and rubbing the surface of inorganic layered bulk materials. The weak van der Waals interaction between the layers of the materials is the key factor so that the applied mechanical force can peel of single or few layers of 2D

materials without breaking the chemical bonding of the in-plane layer. The micromechanical cleavage technique is first used by Grim et al. to obtain graphene monolayer from highly oriented graphite [92]. Besides, a more thin flake can be obtained by repeated several times of this process. Then these thin flakes are washed with acetone and transferred on a clean, flat target surface of SiO₂/Si or quartz to further cleave it using plastic tweezers. The extension of this method have been widely employed to obtain various kinds of ultrathin 2D nanosheets from the bulk materials, such as h-BN [93], various TMD monolayers (TiS₂, TaS₂, MoS₂, WS₂, ReS₂, TaSe₂, NbSe₂, WTe₂, Mo_xW_{1-x}S₂, ReS_{2x}Se_{2(1-x)}, etc.) [94][95][96][97][98][99][100][101][102], topological insulators of Bi₂Te₃, Bi₂Se₃ [103][104], metal phosphorus trichalcogenides of MPS₃ (M = Fe, Ni, Zn, Mn and Cd) [105], BP [106][107] and CuInP₂S₆ [108].

This micromechanical cleavage technique is simple, fast, and low cost, and the size of exfoliated 2D materials can be up to tens of micrometers. Besides, no chemicals are utilized but the shear force is applied during the fabrication process. Thus, the fabricated nanosheets keep the pristine structural integrity with minimum defects from the parental bulk materials, giving rise to many advantages. As a whole, the large lateral size, clean surface, "perfect" crystal quality, high crystallinity make mechanically cleaved 2D materials as remarkable candidates to investigate the corresponding mechanical, electronic, and optical properties and application in electronic and optoelectronic devices. While there are some certain disadvantages that hinder their realistic applications. First, the production yield of this process is extremely low and the nanosheets always coexist with thick flakes on the substrate. Thus, it is suitable for laboratory scale studies but difficult to utilize in various high-end technological applications, high yield, and large-scale production. Second, the fundamental/intrinsic properties, such as size, thickness, and shape of the ultrathin 2D nanosheets are unstable and uncontrollable since the mechanical exfoliation technique by hand is a shortage of precision and repeatability. Third, the utilized substrate is significantly important in the fabrication process. Recently, one advanced micromechanical cleavage method is reported by Sutter et al. to improve the production yield and increase the surface area of graphene and Bi₂Sr₂CaCu₂O_x nanosheets [109]. The first significant key is using oxygen plasma to remove the ambient adsorbates on the substrate. Then a heat treatment is introduced during the fabrication process, which leads to a homogeneous interaction between the substrate and the crystal material [109]. Theoretically speaking, this advanced method can be further used to produce all kinds of ultrathin 2D nanosheets with larger areas and enhanced production yield. Additionally, the evaporation of Au films onto SiO₂/Si before exfoliation is reported previously to enhance the surface area of TMD monolayers since the interaction between Au and chalcogen layer is stronger, giving rise to a stronger contact between the substrate and TMD matrix process, which leads to a homogeneous interaction between the substrate and the crystal material [110].

4.2 Liquid exfoliation

Liquid exfoliation actually also relies on the mechanical forces since the original idea of this technique is to apply the proper mechanical force on layered bulk crystals dispersed in a liquid to exfoliate them into single- or few-layer 2D nanosheets. Thus this technique is mechanical force-assisted liquid exfoliation which can categorize into sonication-assisted liquid exfoliation and shear force-assisted liquid exfoliation. Compare to mechanical exfoliation of 2D nanosheets, liquid exfoliation is a reliable method with high quality and large quantity to produce mono and

few-layer 2D sheets at bulk scale. Up to now, the exfoliation method in liquid media has been largely reported to gain ultrathin 2D materials from their parental layered bulk crystals, such as MoS₂, WS₂, Bi₂Te₃, MoSe₂, NbSe₂, TeSe₂, *h*-BN, NiTe₂, MoTe₂, and so on [111][112][113].

Sonication-assisted liquid exfoliation is an established technique using the simple and common mechanical force to peel the layered bulk materials into 2D sheets in liquid media, in which the bulk crystals are dispersed into a polar solvent and washed using bubbles induced by sonication in the solution. The cavitation bubbles generated by high energy ultrasonic waves could create high energy during the sudden burst with the release of pressure, hence the resultant dispersion is centrifuged to exfoliate of layers in the solution. It is to be noted that the key parameter is the surface energies between the layered bulk materials and the liquid system should be matched. It is because the solvents have the surface tension, using the surface tension of solvent similar to the surface energy of layer bulk crystals could reduce the energetic cost of exfoliation and prohibited the restacking and aggregating between the 2D layers [82][111][114]. For example, it is reported that pure water or pure ethanol is not an efficient way to synthesize TMDs nanosheets due to the large surface energy of the solvent, but the mixing water with ethanol could effectively exfoliate and disperse TMDs. Thus, choosing the optimum solvent could largely utilize the potential of this technique. Besides, the sonication time and centrifugation rate are also significant factors that are related to the quality and quantity of 2D materials. This method is first used to exfoliate graphite into graphene in 2008 [115]. They reported no complicated equipment or expensive chemicals is used during their experiment. Subsequently, more than 25 solvents were studied to naturally exfoliate of 2D nanosheets based on crystallinity, thickness, size, and yield of the resultant layers [111]. It is summarized that dimethylformamide, cyclohexylpyrrolidinone, N-methyl-pyrrolidone, Ndodecyl-pyrrolidone, MDSO, NVP, ortho-dichlorobenzene, and IPA are mostly used solvents to ultrasonic exfoliate of MoS₂, WS₂, VS₂, *h*-BN and MoTe₂ [111][116][117][118]. The sonication-assisted liquid exfoliation with high effectivity and simple method without complex equipment applied has paved a new way to large scale and high yield exfoliation of layered materials into ultrathin 2D monolayers.

Although the production of 2D nanosheets is increased with concentrations of $\sim 1 \text{ mg mL}^{-1}$ by using the sonication-assisted liquid exfoliation method compared to the mechanical cleavage method, the producing rate does not reach the industrial application's requirement. Hence the shear force-assisted liquid exfoliation method is proposed to further enhance the production rate of 2D nanosheets. Coleman et al. found that a high-shear rotor-stator mixer could create high shear rates in a solvent containing bulk layered materials [119][120]. Similarly, the suitable solvent and polymer could minimize the exfoliation energy and stabilize the synthesized 2D nanosheets, leading to the exfoliation process more efficient. The shear-force device is set using a rotor and a stator to form a mixing head, which could exfoliate graphite into graphene with a lateral size of 300-800 nm in N-methyl-pyrrolidone [120]. Particularly, the volume of graphene production can be adjusted by tuning the size of the rotor. Therefore, the effects of rotor size and property of mixer-induced shear force were comprehensively studied previously [121]. It is demonstrated the exfoliation of the bulk layered crystals is highly controlled by the shear rate that if it is lower than 10^4 S^{-1} , the production efficiency would be lower. However, when the shear rate is large than 10^4 S^{-1} , the exfoliation efficiency of graphene will be largely improved [121]. Broadly speaking, the production rate of graphene nanosheets is not only related to the rotor speed, but also with the nanomaterial concentration, volume of solution, and mixing time. Currently, the production rate of graphene could reach up to 1.44 g h^{-1} with a thickness of 2-12

layers and a length of 40-200 nm. These results demonstrate the commercial potential application of shear force-assisted liquid exfoliation method for the high-yield and large-scale production of graphene.

4.3 Chemical vapor deposition

The chemical vapor deposition (CVD) technique is a common and traditional method to synthesize a high-purity 2D layer of metal with large area and uniform thickness, such as Ti, W, Zr, and Si on substrates, for large-scale electronic and flexible optoelectronic devices [122]. The CVD technique is first commercially applied in 1897 to reduce WO_6 in order to coat pure W on carbon filament [123]. Over the past decade, the highly purified polycrystalline Si has been largely produced using the CVD method in the industry. Besides, the CVD method is already a reliable and developed technique for the massive production of the number of ultrathin nanosheets [122]. The growth of few-layer graphene on polycrystalline Ni film by CVD method was first reported by Somani et al. in 2006 [124]. Subsequently, a graphene monolayer is obtained by the CVD technique on a Ni film deposited on SiO_2/Si substrate [125]. Here, not only the Ni film played a role of the substrate to support the growth of graphene, but also acted as a catalyst to promote the formation of precursors to nuclear graphene sheets. Notably, the precursors, Ni film deposited on SiO_2/Si substrate, temperature, catalysts, and atmospheres are the critical parameters to determine the structure-property of graphene in CVD growth [126]. Thus, the production of graphene with controlled layer number, size, and crystallinity can be obtained by optimized those experimental parameters by the CVD method [125][126]. Similarly, the growth of a large number of 2D nanosheets is achieved on different substrates with different precursors in the CVD growth, including h -BN [127], Bi_2Se_3 [128], In_2Se_3 [129], borophenes [130], metal carbides [131][132] and silicene [133]. Taking MoS_2 nanosheets as an example, the first Mo metal film was deposited on SiO_2 substrate by an e-beam evaporator. Then S atoms were heated to 750 °C to generate vapor to react with Mo metal film to form large-area few-layer MoS_2 nanosheets [134]. In addition, controlling the thickness of the Mo thin layer as well as the size of the substrate could roughly adjust the size and thickness of MoS_2 . Until now, MoS_2 , WS_2 , ZrS_2 , ReS_2 , $MoSe_2$, WSe_2 , and so on have been successfully synthesized using the CVD technique on different substrates under different temperatures and atmosphere [134][135][136][137][138][139]. Besides, the CVD method exhibits the highest control ability than other synthetic methods to obtain 2D nanosheets with high crystal quality, high purity. Thus 2D nanomaterials synthesized by the CVD method are ideal candidates for the fabrication of high-performance electronic devices. More importantly, the CVD technique shows promising potential to produce ultrathin 2D sheets on an industrial scale with high yield and high production rate. However, the growth of 2D sheets by the CVD method should be deposited on substrates under high temperatures and inert atmosphere, giving rise up to an expensive cost.

4.4 Van der Waal epitaxial growth on the substrate

There is one important synthesized form for the CVD method, it is van der Waal epitaxial growth on the substrate in which the substrate surface usually plays as a seed crystal. While it is known the substrate often acts as a catalyst. The most predominant of van der Waal epitaxial growth on the substrate is to grow large aspect ratio 2D nanosheets. The epitaxial growth of atom thick, in-plane heterostructure of graphene, and h -BN was reported previously by Liu et al. [140]. Surprisingly, the orientation of h -BN material was dominantly decided by graphene.

Besides, this method was employed under UHV condition with the pressure of 4×10^{-1} torrs to fabricate periodically rippled graphene and islands on Ru(0001) by Vazquez de Parga et al. [141]. In this experiment, the C_2H_4 molecules are used as a precursor, while Ru is a substrate. Detailly, graphene monolayers are prepared by thermal decomposition of C_2H_4 at 1000 K, which is pre-adsorbed on Ru substrate [141]. Besides, it is demonstrated that single-crystalline Ir can also be used as substrates for the synthesis of the high-quality atom thick, large-area graphene monolayer [141]. Recent studies have proven that some 2D heteronanostructures can be obtained by van der Waal epitaxial growth of another TMDs on existing TMD nanosheets, such as WSe_2/WS_2 , $MoSe_2/MoS_2$, and MoS_2/WSe_2 [142][143][144][145]. Importantly, it is demonstrated van der Waal epitaxial modes of lateral and vertical growth can be finely controlled to growth TMD heteronanostructures by adjusting the experimental conditions in the CVD technique [145]. The obtained lateral and vertical specifications are considered as a kind of p-n junctions due to the different band gaps of different ultrathin 2D TMDs, which are promising candidates for utilizing in high-performance electronic devices as electronics or optoelectronics [146].

4.5 Hydrothermal synthesis

Hydrothermal synthesis is another popular bottom-up method to crystallize substance at high pressure and high temperature. Particularly, it is suitable to synthesize the materials which possess high vapor pressure at the melting point. Besides, layered 2D nanosheets could be synthesized using the hydrothermal method. Taking MoS_2 as an example, MoO_3 or ammonium molybdate as the precursor of Mo and sulfur powder or potassium thiocyanate (KSCN) as the precursor of S are dissolved in a hydrazine monohydrate solvent at 150-180 °C for 48 h to fully chemical reaction, then Mo_2 and $MoSe_2$ monolayer can be initially synthesized and aggregated to form nanoflowers or nanotubes [147]. It is worth to mention there is no tendency to restack in Mo_2 and $MoSe_2$ monolayers if not use a surfactant. In addition, there are more intrinsic defects on TMDs are by employing excess thiourea as a precursor to form the 2D nanosheets, which could provide more active sites of TMDs for catalytic applications [148]. Furthermore, Xie et al. applied the hydrothermal method to obtain O incorporated MoS_2 monolayer in the water at 200 °C with the interlayer spacing of 9.5 Å, which is larger than 6.15 Å of pristine MoS_2 [149]. On the other hand, hydrothermal synthesis could generate a hybrid 1T/2H phase in the existing MoS_2 monolayers by a second solvothermal treatment [150]. The mixed 2H and 1T phase of MoS_2 nanosheets shows a robust ferromagnetism feature at room temperature due to the metallic property of 1T MoS_2 monolayer. Subsequently, the hydrothermal-solvothermal approach is widely used to fabric hybridization MoS_2 -based adsorbents with other functional nanosheets, such as nano- Fe_3O_4 [151]. Groups IV and V transition metal chalcogenides from metal chloride can also be obtained hydrothermally/solvothermal in oleylamine [152]. CS_2 is used as the source of S atoms since it could produce H_2S which could further react with the precursor of groups IV or V transition metal to form metal disulfides nanomaterials. Moreover, CSe_2 , the precursor of Se gives a better layered crystalline structure than CS_2 due to the high structural stability of CSe_2 [152][153].

The hydrothermal method is recently widely used in industrial incubation to large-scale synthesize nanosheets. For example, *h*-BN can be largely produced at 500 °C using boric anhydride, Zn powder, and $N_2H_2 \cdot 2HCl$ or boric acid and urea at 900 °C [154]. Besides TMDs, transition metal oxides and hydroxides have been extensively prepared on the gram scale via utilizing the hydrothermal method. Eu doped yttrium hydroxide nanomaterials can also be

obtained hydrothermally/solvothermal using triethylamine as an alkaline and complexing source [155]. The VO₂ nanoribbons were prepared under the hydrothermal reduction of V₂O₅ and graphene oxide. The thickness, width, and length of VO₂ nanosheets could reach up to ~10 nm, 50-500 nm, and ~10 μm, respectively, which could be used as the cathode in lithium-ion batteries [156]. The more complex composites of FeNi₂S₄-graphene-MoS₂ and FeNi₂S₄-graphene-MoSe₂ can also be synthesized by using the hydrothermal method [157][158]. The hydrothermal synthesis method has a lot of advantages to synthesize ultrathin 2D nanosheets due to the process is simple, stable, and scalable. Whereas, the micro growth mechanism of the hydrothermal method is hard to figure out in that the whole reaction has happened in a sealed autoclave. More important, the hydrothermal synthesis method is very sensitive to the concentration of precursors, solvent system, temperature as well as whether using surfactants or polymers, so it is difficult to design an experiment to produce other 2D nanosheets.

5. Conclusions, Perspectives, and Challenges

In summary, we have attempted to provide a panorama of basic principles and mechanisms with regard to improving the structure stability, physical and chemical properties of low dimensional semiconductor-based photocatalysts. After reporting on a large amount of literature, various 2D semiconductor-based photocatalysts show a high electrochemical property and photocatalytic performance due to their ultrathin character, high specific surface area with more activity sites, tunable bandgap to absorb sunlight, and versatile options in structural assembly with other nanosheets. Particularly, special focus has been placed on various strategies implemented to tackle problems associated with synthetic methods, structural stability, and property, durability, and photodecomposition of 2D semiconductors. From the above, one can know extensive efforts have been devoted in the last few decades to construct various photocatalytic 2D semiconductors. Yet, co-photocatalysts made up of earth-abundant elements with low-cost are still required to further investigate and develop a mechanistic understanding and controllable synthetic strategy in order to achieve high-efficiency, stable, and less costly 2D semiconductor-based photocatalysts. Many challenges, such as the low yield efficiency, stability, durability against etchant solution, kinetics of charge carriers absorption and migration, charge trap, and recycling demand, need to be settled urgently in the near future.

Concurrently, advanced methods for tailoring the electronic and chemical structures of these 2D semiconductor materials have been developed, pushing its rapid development in various photocatalytic applications. For example, homogeneous doping has become a reality [66][159], but how to identify the dopant-induced electronic structures and what is the effect of doping elements on the stability of the system under reaction conditions are rarely being investigated. Until now, only a few examples of improved photocatalyst stability of photocatalysts have been reported in order to deal with the complicated synthetic processes during splitting water. Thus, the present studies on 2D semiconductor photocatalysts are still in the initial stage and further systematic investigations are required. On the other hand, in order to precisely control the dopant distribution, uniformity, composition and the surface states property of photocatalysts, seeking new doping approaches should be addressed for efficient photocatalyst design. In addition, the influence of intrinsic defects, structural shape, the number of layers, and lateral interface size is barely evaluated on the photocatalytic performance, especially in composite photocatalysts. Importantly, an

overall apparent efficiency of the entire photocatalytic system is the main topic in the current studies. While the charge transfer process, such as transfer minimum energy pathways, migration diffusivity, charge carrier lifetime recombination reason, etc., in photocatalysts should be addressed and detailedly investigated to further advance the field. With regard to the recycling problem, designing suitable devices or tuning the magnetic properties might be a good choice.

In the theoretical aspect, first-principles calculations based on density functional theory (DFT) are an efficient way to screen the photocatalytic potential spaces, however, a number of key bottlenecks are required to breakthrough. Firstly, the solvation effects are not considered in most of the present theoretical studies. Whereas it is well known that most photocatalytic reactions are related to solid-liquid reaction systems. Hence, it is significantly important and necessary to develop an accurate solvation model as realistically as possible. For example, how the various molecules adsorb on the photocatalyst and influence the calculation of reaction energy and energy barrier heights should be considered in the photocatalyst system in order to realistically simulate the experimental testing conditions. Secondly, various previous theoretical data use the traditional DFT method, whereas the enlightenment of photocatalytic kinetic studies is still rarely studied due to the fact that it is technically challenging. The photoexcitation of a semiconductor photocatalyst, including 1D, 2D, and 3D materials, produces photogenerated electrons and holes, leading to an excited state of the photocatalyst. However, the feature of the excited state and the corresponding reason for the energy barrier reduction under light irradiation are still secrets. Therefore, understanding the dynamics of excited electrons plays a significant role in understanding the whole photocatalytic processes [\[160\]](#)[\[161\]](#). Thirdly, the thermodynamic photocatalytic processes, such as energetic requirement, band edge alignment relative to the hydrogen revolution potential of H_2/H^+ , and oxygen revolution potential of H_2O/O_2 needs to be deeply understood. For example, the migration behaviors of electrons and holes from substrates are not given much attention, which exhibits significant impacts on photocatalytic efficiency since 2D atomic thin photocatalysts are usually stabilized on various substrates. Last but not least, novel simulation methods or performing dynamic simulation algorithms rather than static crystal models are strongly required since the surfaces of photocatalysts are dynamically and frequently undergoing changes during the reaction proceeds. With rapid advances and rich knowledge about 2D materials in the many joint efforts of research and development sectors in the last few decades, it is the best time for us to do research on photocatalysis. At the same time, one can envision that utilization of the absorbed sunlight energy could largely reduce the fossil energy demand for human development, and further decrease the environmental pollution. Thus one can see photocatalysts play an increasingly important role in that we not only need to improve the performance of the existing photocatalysts but also invent new engineering approaches to better exploit new novel photocatalysts. Thus, joint efforts from various disciplines are needed. We wish that the present mini-review serves as a catalyst to facilitate the discussions by various specialists from physics, chemistry, materials engineering, computer science, and so on.

References

1. Conti, J.; Holtberg, P.; Diefenderfer, J.; LaRose, A.; Turnure, J.T.; Westfall, L. International Energy Outlook 2016 with Projections to 2040; Technical Report; USDOE Energy Information Administration (EIA): Washington, DC, USA, 2016; Office of Energy Analysis.
2. Yang, X.; Yang, Y.; Lu, Y.; Sun, Z.; Hussain, S.; Zhang, P. First-principles GGA+U calculation investigating the hydriding and diffusion properties of hydrogen in PuH_{2+x} , $0 \leq x \leq 1$. *Int. J. Hydrogen Energy* 2018, 43, 13632–13638.
3. Qu, Y.; Duan, X. Progress, challenge and perspective of heterogeneous photocatalysts. *Chem. Soc. Rev.* 2013, 42, 2568–2580.
4. Colmenares, J.C.; Luque, R.; Campelo, J.M.; Colmenares, F.; Karpiński, Z.; Romero, A.A. Nanostructured photocatalysts and their applications in the photocatalytic transformation of lignocellulosic biomass: An overview. *Materials* 2009, 2, 2228–2258.
5. Yang, X.; Lu, Y.; Zhang, P. First-principles study of native point defects and diffusion behaviors of helium in zirconium carbide. *J. Nucl. Mater.* 2015, 465, 161–166.
6. Graetzel, M. Artificial photosynthesis: Water cleavage into hydrogen and oxygen by visible light. *Accounts Chem. Res.* 1981, 14, 376–384.
7. Walter, M.G.; Warren, E.L.; McKone, J.R.; Boettcher, S.W.; Mi, Q.; Santori, E.A.; Lewis, N.S. Solar water splitting cells. *Chem. Rev.* 2010, 110, 6446–6473.
8. Armelao, L.; Barreca, D.; Bottaro, G.; Gasparotto, A.; Maccato, C.; Maragno, C.; Tondello, E.; Štangar, U.L.; Bergant, M.; Mahne, D. Photocatalytic and antibacterial activity of TiO_2 and Au/TiO_2 nanosystems. *Nanotechnology* 2007, 18, 375709.
9. Folli, A.; Pade, C.; Hansen, T.B.; De Marco, T.; Macphee, D.E. TiO_2 photocatalysis in cementitious systems: Insights into self-cleaning and depollution chemistry. *Cement Concrete Res.* 2012, 42, 539–548.
10. Yue, X.Q. Effect of ZnO-loading method on adsorption and decomposition capacities of expanded graphite/ZnO composites for crude oil. *Adv. Mater. Res. Trans. Tech. Publ.* 2011, 284, 173–176.
11. Kwon, S.; Fan, M.; Cooper, A.T.; Yang, H. Photocatalytic applications of micro- and nano- TiO_2 in environmental engineering. *Crit. Rev. Environ. Sci. Technol.* 2008, 38, 197–226.
12. Cai, R.; Hashimoto, K.; Kubota, Y.; Fujishima, A. Increment of photocatalytic killing of cancer cells using TiO_2 with the aid of superoxide dismutase. *Chem. Lett.* 1992, 21, 427–430.
13. Tian, C.Y.; Xu, J.J.; Chen, H.Y. A novel aptasensor for the detection of adenosine in cancer cells by electrochemiluminescence of nitrogen doped TiO_2 nanotubes. *Chem. Commun.* 2012, 48, 8234–8236.
14. Kudo, A.; Miseki, Y. Heterogeneous photocatalyst materials for water splitting. *Chem. Soc. Rev.* 2009, 38, 253–278.

15. Ganguly, P.; Byrne, C.; Breen, A.; Pillai, S.C. Antimicrobial activity of photocatalysts: Fundamentals, mechanisms, kinetics and recent advances. *Appl. Catal. B Environ.* 2018, 225, 51–75.
16. Yalavarthi, R.; Naldoni, A.; Kment, Š.; Mascaretti, L.; Kmentová, H.; Tomanec, O.; Schmuki, P.; Zbořil, R. Radiative and non-radiative recombination pathways in mixed-phase TiO₂ nanotubes for PEC water-splitting. *Catalysts* 2019, 9, 204.
17. Fujishima, A.; Honda, K. Electrochemical photolysis of water at a semiconductor electrode. *Nature* 1972, 238, 37–38.
18. Yuan, Y.J.; Chen, D.; Yu, Z.T.; Zou, Z.G. Cadmium sulfide-based nanomaterials for photocatalytic hydrogen production. *J. Mater. Chem. A* 2018, 6, 11606–11630.
19. Tong, H.; Ouyang, S.; Bi, Y.; Umezawa, N.; Oshikiri, M.; Ye, J. Nano-photocatalytic materials: Possibilities and challenges. *Nat. Rev. Mater.* 2012, 24, 229–251.
20. Zhang, N.; Wang, L.; Wang, H.; Cao, R.; Wang, J.; Bai, F.; Fan, H. Self-assembled one-dimensional porphyrin nanostructures with enhanced photocatalytic hydrogen generation. *Nano Lett.* 2018, 18, 560–566.
21. Ma, Y.; Wang, X.; Jia, Y.; Chen, X.; Han, H.; Li, C. Titanium dioxide-based nanomaterials for photocatalytic fuel generations. *Chem. Rev.* 2014, 114, 9987–10043.
22. Che, W.; Cheng, W.; Yao, T.; Tang, F.; Liu, W.; Su, H.; Huang, Y.; Liu, Q.; Liu, J.; Hu, F.; et al. Fast photoelectron transfer in (Cring)-C₃N₄ plane heterostructural nanosheets for overall water splitting. *J. Am. Chem. Soc.* 2017, 139, 3021–3026.
23. Cai, X.; Zhu, M.; Elbanna, O.A.; Fujitsuka, M.; Kim, S.; Mao, L.; Zhang, J.; Majima, T. Au nanorod photosensitized La₂Ti₂O₇ nanosteps: Successive surface heterojunctions boosting visible to near-infrared photocatalytic H₂ evolution. *ACS Catal.* 2018, 8, 122–131.
24. Singh, D.; Panda, P.K.; Khossossi, N.; Mishra, Y.K.; Ainane, A.; Ahuja, R. Impact of edge structures on interfacial interactions and efficient visible-light photocatalytic activity of metal–semiconductor hybrid 2D materials. *Catal. Sci. Technol.* 2020, 10, 3279–3289.
25. Singh, D.; Chakraborty, S.; Ahuja, R. Emergence of Si₂BN Monolayer as Efficient HER Catalyst under Co-functionalization Influence. *ACS Appl. Energy Mater.* 2019, 2, 8441–8448.
26. Hartley, C.L.; DiRisio, R.J.; Screen, M.E.; Mayer, K.J.; McNamara, W.R. Iron polypyridyl complexes for photocatalytic hydrogen generation. *Inorg. Chem.* 2016, 55, 8865–8870.
27. Zhang, L.Y.; Yin, S.Y.; Pan, M.; Liao, W.M.; Zhang, J.H.; Wang, H.P.; Su, C.Y. Binuclear Ru–Ru and Ir–Ru complexes for deep red emission and photocatalytic water reduction. *J. Mater. Chem. A* 2017, 5, 9807–9814.

28. Greene, B.L.; Schut, G.J.; Adams, M.W.; Dyer, R.B. Pre-Steady-State Kinetics of Catalytic Intermediates of an [FeFe]-Hydrogenase. *ACS Catal.* 2017, 7, 2145–2150.
29. Singh, D.; Gupta, S.K.; Sonvane, Y.; Kumar, A.; Ahuja, R. 2D-HfS₂ as an efficient photocatalyst for water splitting. *Catal. Sci. Technol.* 2016, 6, 6605–6614.
30. Zhao, X.; Yang, X.; Singh, D.; Panda, P.K.; Luo, W.; Li, Y.; Ahuja, R. Strain-Engineered Metal-Free h-B₂O Monolayer as a Mechanocatalyst for Photocatalysis and Improved Hydrogen Evolution Reaction. *J. Phys. Chem. C* 2020, 124, 7884–7892.
31. Hutton, G.A.; Reuillard, B.; Martindale, B.C.; Caputo, C.A.; Lockwood, C.W.; Butt, J.N.; Reisner, E. Carbon dots as versatile photosensitizers for solar-driven catalysis with redox enzymes. *J. Am. Chem. Soc.* 2016, 138, 16722–16730.
32. Lv, H.; Ruberu, T.P.A.; Fleischauer, V.E.; Brennessel, W.W.; Neidig, M.L.; Eisenberg, R. Catalytic light-driven generation of hydrogen from water by iron dithiolene complexes. *J. Am. Chem. Soc.* 2016, 138, 11654–11663.
33. Yuan, Y.J.; Chen, D.Q.; Xiong, M.; Zhong, J.S.; Wan, Z.Y.; Zhou, Y.; Liu, S.; Yu, Z.T.; Yang, L.X.; Zou, Z.G. Bandgap engineering of (AgIn)_xZn₂(1-x)S₂ quantum dot photosensitizers for photocatalytic H₂ generation. *Appl. Catal. B Environ.* 2017, 204, 58–66.
34. Sakai, T.; Mersch, D.; Reisner, E. Photocatalytic hydrogen evolution with a hydrogenase in a mediator-free system under high levels of oxygen. *Angew. Chem.* 2013, 52, 12313–12316.
35. Han, Z.; Shen, L.; Brennessel, W.W.; Holland, P.L.; Eisenberg, R. Nickel pyridinethiolate complexes as catalysts for the light-driven production of hydrogen from aqueous solutions in noble-metal-free systems. *J. Am. Chem. Soc.* 2013, 135, 14659–14669.
36. Yuan, Y.J.; Lu, H.W.; Tu, J.R.; Fang, Y.; Yu, Z.T.; Fan, X.X.; Zou, Z.G. A Noble-Metal-Free Nickel (II) Polypyridyl Catalyst for Visible-Light-Driven Hydrogen Production from Water. *ChemPhysChem* 2015, 16, 2925–2930.
37. Kagalwala, H.N.; Chirdon, D.N.; Mills, I.N.; Budwal, N.; Bernhard, S. Light-driven hydrogen generation from microemulsions using metallosurfactant catalysts and oxalic acid. *Inorg. Chem.* 2017, 56, 10162–10171.
38. Yuan, Y.J.; Ye, Z.J.; Lu, H.W.; Hu, B.; Li, Y.H.; Chen, D.Q.; Zhong, J.S.; Yu, Z.T.; Zou, Z.G. Constructing anatase TiO₂ nanosheets with exposed (001) facets/layered MoS₂ two-dimensional nanojunctions for enhanced solar hydrogen generation. *ACS Catal.* 2016, 6, 532–541.
39. Lin, Z.; Xiao, J.; Li, L.; Liu, P.; Wang, C.; Yang, G. Nanodiamond-Embedded p-Type Copper (I) Oxide Nanocrystals for Broad-Spectrum Photocatalytic Hydrogen Evolution. *Adv. Energy Mater.* 2016, 6, 1501865.

40. Wang, Q.; Hisatomi, T.; Jia, Q.; Tokudome, H.; Zhong, M.; Wang, C.; Pan, Z.; Takata, T.; Nakabayashi, M.; Shibata, N.; et al. Scalable water splitting on particulate photocatalyst sheets with a solar-to-hydrogen energy conversion efficiency exceeding 1%. *Nat. Mater.* 2016, 15, 611–615.
41. Liu, L.; Peter, Y.Y.; Chen, X.; Mao, S.S.; Shen, D. Hydrogenation and disorder in engineered black TiO₂. *Phys. Rev. Lett.* 2013, 111, 065505.
42. Xu, M.; Gao, Y.; Moreno, E.M.; Kunst, M.; Muhler, M.; Wang, Y.; Idriss, H.; Wöll, C. Photocatalytic activity of bulk TiO₂ anatase and rutile single crystals using infrared absorption spectroscopy. *Phys. Rev. Lett.* 2011, 106, 138302.
43. Li, X.; Li, Z.; Yang, J. Proposed photosynthesis method for producing hydrogen from dissociated water molecules using incident near-infrared light. *Phys. Rev. Lett.* 2014, 112, 018301.
44. Ahmed, M.; Guo, X. A review of metal oxynitrides for photocatalysis. *Inorg. Chem. Front.* 2016, 3, 578–590.
45. Yang, X.; Banerjee, A.; Ahuja, R. Probing the active sites of newly predicted stable Janus scandium dichalcogenides for photocatalytic water-splitting. *Catal. Sci. Technol.* 2019, 9, 4981–4989.
46. Serpone, N.; Emeline, A.; Ryabchuk, V.; Kuznetsov, V. Why do hydrogen and oxygen yields from semiconductor-based photocatalyzed water splitting remain disappointingly low? Intrinsic and extrinsic factors impacting surface redox reactions. *ACS Energy Lett.* 2016, 1, 931–948.
47. Fukuzumi, S.; Hong, D.; Yamada, Y. Bioinspired photocatalytic water reduction and oxidation with earth-abundant metal catalysts. *J. Phys. Chem. Lett.* 2013, 4, 3458–3467.
48. Guzman, F.; Chuang, S.S.; Yang, C. Role of methanol sacrificing reagent in the photocatalytic evolution of hydrogen. *Ind. Eng. Chem. Res.* 2013, 52, 61–65.
49. Salzl, S.; Ertl, M.; Knör, G. Evidence for photosensitized hydrogen production from water in the absence of precious metals, redox-mediators and co-catalysts. *Phys. Chem. Chem. Phys.* 2017, 19, 8141–8147.
50. Simon, T.; Bouchonville, N.; Berr, M.J.; Vaneski, A.; Adrović, A.; Volbers, D.; Wyrwich, R.; Döblinger, M.; Susha, A.S.; Rogach, A.L.; et al. Redox shuttle mechanism enhances photocatalytic H₂ generation on Ni-decorated CdS nanorods. *Nat. Mater.* 2014, 13, 1013–1018.
51. Wang, J.; Chen, Y.; Zhou, W.; Tian, G.; Xiao, Y.; Fu, H.; Fu, H. Cubic quantum dot/hexagonal microsphere ZnIn₂S₄ heterophase junctions for exceptional visible-light-driven photocatalytic H₂ evolution. *J. Mater. Chem. A* 2017, 5, 8451–8460.
52. Wang, X.; Maeda, K.; Thomas, A.; Takanabe, K.; Xin, G.; Carlsson, J.M.; Domen, K.; Antonietti, M. A metal-free polymeric photocatalyst for hydrogen production from water under visible light.

- Nat. Mater. 2009, 8, 76–80.
53. Han, Z.; Qiu, F.; Eisenberg, R.; Holland, P.L.; Krauss, T.D. Robust photogeneration of H₂ in water using semiconductor nanocrystals and a nickel catalyst. *Science* 2012, 338, 1321–1324.
 54. Xu, J.; Cao, X. Characterization and mechanism of MoS₂/CdS composite photocatalyst used for hydrogen production from water splitting under visible light. *Chem. Eng. J.* 2015, 260, 642–648.
 55. Kim, W.; Tachikawa, T.; Majima, T.; Li, C.; Kim, H.J.; Choi, W. Tin-porphyrin sensitized TiO₂ for the production of H₂ under visible light. *Energy Environ. Sci.* 2010, 3, 1789–1795.
 56. Ye, C.; Li, J.X.; Li, Z.J.; Li, X.B.; Fan, X.B.; Zhang, L.P.; Chen, B.; Tung, C.H.; Wu, L.Z. Enhanced driving force and charge separation efficiency of protonated g-C₃N₄ for photocatalytic O₂ evolution. *ACS Catal.* 2015, 5, 6973–6979.
 57. Asahi, R.; Morikawa, T.; Ohwaki, T.; Aoki, K.; Taga, Y. Visible-light photocatalysis in nitrogen-doped titanium oxides. *Science* 2001, 293, 269–271.
 58. Yang, X.; Banerjee, A.; Xu, Z.; Wang, Z.; Ahuja, R. Interfacial aspect of ZnTe/In₂Te₃ heterostructures as an efficient catalyst for the hydrogen evolution reaction. *J. Mater. Chem. A* 2019, 7, 27441–27449.
 59. Wen, C.Z.; Hu, Q.H.; Guo, Y.N.; Gong, X.Q.; Qiao, S.Z.; Yang, H.G. From titanium oxydifluoride (TiOF₂) to titania (TiO₂): Phase transition and non-metal doping with enhanced photocatalytic hydrogen (H₂) evolution properties. *Chem. Commun.* 2011, 47, 6138–6140.
 60. Yu, J.; Zhang, J.; Jaroniec, M. Preparation and enhanced visible-light photocatalytic H₂-production activity of CdS quantum dots-sensitized Zn_{1-x}Cd_xS solid solution. *Green Chem.* 2010, 12, 1611–1614.
 61. Ning, Z.; Tian, H.; Yuan, C.; Fu, Y.; Qin, H.; Sun, L.; Ågren, H. Solar cells sensitized with type-II ZnSe–CdS core/shell colloidal quantum dots. *Chem. Commun.* 2011, 47, 1536–1538.
 62. Chen, X.; Liu, L.; Peter, Y.Y.; Mao, S.S. Increasing solar absorption for photocatalysis with black hydrogenated titanium dioxide nanocrystals. *Science* 2011, 331, 746–750.
 63. Thimsen, E.; Le Formal, F.; Gratzel, M.; Warren, S.C. Influence of plasmonic Au nanoparticles on the photoactivity of Fe₂O₃ electrodes for water splitting. *Nano Lett.* 2011, 11, 35–43.
 64. Wu, H.B.; Hng, H.H.; Lou, X.W. Direct synthesis of anatase TiO₂ nanowires with enhanced photocatalytic activity. *Adv. Mater.* 2012, 24, 2567–2571.
 65. Chen, J.S.; Chen, C.; Liu, J.; Xu, R.; Qiao, S.Z.; Lou, X.W. Ellipsoidal hollow nanostructures assembled from anatase TiO₂ nanosheets as a magnetically separable photocatalyst. *Chem. Commun.* 2011, 47, 2631–2633.

66. Meng, F.; Li, J.; Cushing, S.K.; Zhi, M.; Wu, N. Solar hydrogen generation by nanoscale p-n junction of p-type molybdenum disulfide/n-type nitrogen-doped reduced graphene oxide. *J. Am. Chem. Soc.* 2013, 135, 10286–10289.
67. Wang, X.; Xu, Q.; Li, M.; Shen, S.; Wang, X.; Wang, Y.; Feng, Z.; Shi, J.; Han, H.; Li, C. Photocatalytic overall water splitting promoted by an α - β phase junction on Ga₂O₃. *Angew. Chem.* 2012, 124, 13266–13269.
68. Konta, R.; Ishii, T.; Kato, H.; Kudo, A. Photocatalytic Activities of Noble Metal Ion Doped SrTiO₃ under Visible Light Irradiation. *J. Phys. Chem. B* 2004, 108, 8992–8995.
69. Maeda, K.; Teramura, K.; Lu, D.; Takata, T.; Saito, N.; Inoue, Y.; Domen, K. Photocatalyst releasing hydrogen from water. *Nature* 2006, 440, 295.
70. Maeda, K.; Teramura, K.; Lu, D.; Saito, N.; Inoue, Y.; Domen, K. Noble-metal/Cr₂O₃ core/shell nanoparticles as a cocatalyst for photocatalytic overall water splitting. *Angew. Chem.* 2006, 118, 7970–7973.
71. Maeda, K.; Sakamoto, N.; Ikeda, T.; Ohtsuka, H.; Xiong, A.; Lu, D.; Kanehara, M.; Teranishi, T.; Domen, K. Preparation of Core–Shell-Structured Nanoparticles (with a Noble-Metal or Metal Oxide Core and a Chromia Shell) and Their Application in Water Splitting by Means of Visible Light. *Chem. Eur. J.* 2010, 16, 7750–7759.
72. Qu, Y.; Liao, L.; Cheng, R.; Wang, Y.; Lin, Y.C.; Huang, Y.; Duan, X. Rational design and synthesis of freestanding photoelectric nanodevices as highly efficient photocatalysts. *Nano Lett.* 2010, 10, 1941–1949.
73. Yang, Z.; Zhang, J.; Kintner-Meyer, M.C.; Lu, X.; Choi, D.; Lemmon, J.P.; Liu, J. Electrochemical energy storage for green grid. *Chem. Rev.* 2011, 111, 3577–3613.
74. Zhou, H.; Qu, Y.; Zeid, T.; Duan, X. Towards highly efficient photocatalysts using semiconductor nanoarchitectures. *Energy Environ. Sci.* 2012, 5, 6732–6743.
75. Hochbaum, A.I.; Yang, P. Semiconductor nanowires for energy conversion. *Chem. Rev.* 2010, 110, 527–546.
76. Atwater, H.A.; Polman, A. Plasmonics for improved photovoltaic devices. In *Materials for Sustainable Energy: A Collection of Peer-Reviewed Research and Review Articles from Nature Publishing Group*; World Scientific: Singapore, 2011; pp. 1–11.
77. Tafen, D.N.; Long, R.; Prezhdo, O.V. Dimensionality of nanoscale TiO₂ determines the mechanism of photoinduced electron injection from a CdSe nanoparticle. *Nano Lett.* 2014, 14, 1790–1796.
78. She, X.; Wu, J.; Xu, H.; Zhong, J.; Wang, Y.; Song, Y.; Nie, K.; Liu, Y.; Yang, Y.; Rodrigues, M.T.F.; et al. High efficiency photocatalytic water splitting using 2D α -Fe₂O₃/g-C₃N₄ Z-scheme catalysts.

- Adv. Energy Mater. 2017, 7, 1700025.
79. Han, Q.; Wang, B.; Gao, J.; Cheng, Z.; Zhao, Y.; Zhang, Z.; Qu, L. Atomically thin mesoporous nanomesh of graphitic C₃N₄ for high-efficiency photocatalytic hydrogen evolution. *ACS Nano* 2016, 10, 2745–2751.
80. Sivula, K. Metal oxide photoelectrodes for solar fuel production, surface traps, and catalysis. *J. Phys. Chem. Lett.* 2013, 4, 1624–1633.
81. Hisatomi, T.; Kubota, J.; Domen, K. Recent advances in semiconductors for photocatalytic and photoelectrochemical water splitting. *Chem. Soc. Rev.* 2014, 43, 7520–7535.
82. Nicolosi, V.; Chhowalla, M.; Kanatzidis, M.G.; Strano, M.S.; Coleman, J.N. Liquid exfoliation of layered materials. *Science* 2013, 340, 1226419.
83. Son, J.S.; Yu, J.H.; Kwon, S.G.; Lee, J.; Joo, J.; Hyeon, T. Colloidal Synthesis of Ultrathin Two-Dimensional Semiconductor Nanocrystals. *Adv. Mater.* 2011, 23, 3214–3219.
84. Oh, S.M.; Patil, S.B.; Jin, X.; Hwang, S.J. Recent applications of 2D inorganic nanosheets for emerging energy storage system. *Chem. Eur. J.* 2018, 24, 4757–4773.
85. Zhang, H. Ultrathin two-dimensional nanomaterials. *ACS Nano* 2015, 9, 9451–9469.
86. Voiry, D.; Mohite, A.; Chhowalla, M. Phase engineering of transition metal dichalcogenides. *Chem. Soc. Rev.* 2015, 44, 2702–2712.
87. Fan, Z.; Zhang, H. Crystal phase-controlled synthesis, properties and applications of noble metal nanomaterials. *Chem. Soc. Rev.* 2016, 45, 63–82.
88. Chhowalla, M.; Voiry, D.; Yang, J.; Shin, H.S.; Loh, K.P. Phase-engineered transition-metal dichalcogenides for energy and electronics. *MRS Bull.* 2015, 40, 585.
89. Ambrosi, A.; Sofer, Z.; Pumera, M. 2H → 1T phase transition and hydrogen evolution activity of MoS₂, MoSe₂, WS₂ and WSe₂ strongly depends on the MX₂ composition. *Chem. Commun.* 2015, 51, 8450–8453.
90. Chang, K.; Hai, X.; Pang, H.; Zhang, H.; Shi, L.; Liu, G.; Liu, H.; Zhao, G.; Li, M.; Ye, J. Targeted synthesis of 2H-and 1T-phase MoS₂ monolayers for catalytic hydrogen evolution. *Adv. Mater.* 2016, 28, 10033–10041.
91. Qu, Y.; Medina, H.; Wang, S.W.; Wang, Y.C.; Chen, C.W.; Su, T.Y.; Manikandan, A.; Wang, K.; Shih, Y.C.; Chang, J.W.; et al. Wafer Scale Phase-Engineered 1T-and 2H-MoSe₂/Mo Core–Shell 3D-Hierarchical Nanostructures toward Efficient Electrocatalytic Hydrogen Evolution Reaction. *Nat. Rev. Mater.* 2016, 28, 9831–9838.
92. Novoselov, K.S.; Geim, A.K.; Morozov, S.V.; Jiang, D.; Zhang, Y.; Dubonos, S.V.; Grigorieva, I.V.; Firsov, A.A. Electric field effect in atomically thin carbon films. *Science* 2004, 306, 666–669.

93. Pacile, D.; Meyer, J.; Girit, Ç.; Zettl, A. The two-dimensional phase of boron nitride: Few-atomic-layer sheets and suspended membranes. *Appl. Phys. Lett.* 2008, 92, 133107.
94. Li, H.; Yin, Z.; He, Q.; Li, H.; Huang, X.; Lu, G.; Fam, D.W.H.; Tok, A.I.Y.; Zhang, Q.; Zhang, H. Fabrication of single-and multilayer MoS₂ film-based field-effect transistors for sensing NO at room temperature. *Small* 2012, 8, 63–67.
95. Late, D.J.; Doneux, T.; Bougouma, M. Single-layer MoSe₂ based NH₃ gas sensor. *Appl. Phys. Lett.* 2014, 105, 233103.
96. Li, H.; Lu, G.; Wang, Y.; Yin, Z.; Cong, C.; He, Q.; Wang, L.; Ding, F.; Yu, T.; Zhang, H. Mechanical exfoliation and characterization of single-and few-layer nanosheets of WSe₂, TaS₂, and TaSe₂. *Small* 2013, 9, 1974–1981.
97. Pezeshki, A.; Hosseini Shokouh, S.H.; Jeon, P.J.; Shackery, I.; Kim, J.S.; Oh, I.K.; Jun, S.C.; Kim, H.; Im, S. Static and dynamic performance of complementary inverters based on nanosheet α -MoTe₂ p-channel and MoS₂ n-channel transistors. *ACS Nano* 2016, 10, 1118–1125.
98. Liu, F.; Zheng, S.; He, X.; Chaturvedi, A.; He, J.; Chow, W.L.; Mion, T.R.; Wang, X.; Zhou, J.; Fu, Q.; et al. Highly sensitive detection of polarized light using anisotropic 2D ReS₂. *Adv. Funct. Mater.* 2016, 26, 1169–1177.
99. Dumcenco, D.O.; Kobayashi, H.; Liu, Z.; Huang, Y.S.; Suenaga, K. Visualization and quantification of transition metal atomic mixing in Mo_{1-x}W_xS₂ single layers. *Nat. Commun.* 2013, 4, 1–5.
100. Chen, Y.; Xi, J.; Dumcenco, D.O.; Liu, Z.; Suenaga, K.; Wang, D.; Shuai, Z.; Huang, Y.S.; Xie, L. Tunable band gap photoluminescence from atomically thin transition-metal dichalcogenide alloys. *ACS Nano* 2013, 7, 4610–4616.
101. Chen, Y.; Dumcenco, D.O.; Zhu, Y.; Zhang, X.; Mao, N.; Feng, Q.; Zhang, M.; Zhang, J.; Tan, P.H.; Huang, Y.S.; et al. Composition-dependent Raman modes of Mo_{1-x}W_xS₂ monolayer alloys. *Nanoscale* 2014, 6, 2833–2839.
102. Liu, F.; Zheng, S.; Chaturvedi, A.; Zólyomi, V.; Zhou, J.; Fu, Q.; Zhu, C.; Yu, P.; Zeng, Q.; Drummond, N.D.; et al. Optoelectronic properties of atomically thin ReSSe with weak interlayer coupling. *Nanoscale* 2016, 8, 5826–5834.
103. Goyal, V.; Teweldebrhan, D.; Balandin, A.A. Mechanically-exfoliated stacks of thin films of Bi₂Te₃ topological insulators with enhanced thermoelectric performance. *Appl. Phys. Lett.* 2010, 97, 133117.
104. Shahil, K.; Hossain, M.; Goyal, V.; Balandin, A. Micro-Raman spectroscopy of mechanically exfoliated few-quintuple layers of Bi₂Te₃, Bi₂Se₃, and Sb₂Te₃ materials. *J. Appl. Phys.* 2012, 111, 054305.

105. Du, K.z.; Wang, X.z.; Liu, Y.; Hu, P.; Utama, M.I.B.; Gan, C.K.; Xiong, Q.; Kloc, C. Weak van der Waals stacking, wide-range band gap, and Raman study on ultrathin layers of metal phosphorus trichalcogenides. *ACS Nano* 2016, 10, 1738–1743.
106. Castellanos-Gomez, A.; Vicarelli, L.; Prada, E.; Island, J.O.; Narasimha-Acharya, K.; Blanter, S.I.; Groenendijk, D.J.; Buscema, M.; Steele, G.A.; Alvarez, J.V.; et al. Isolation and characterization of few-layer black phosphorus. *2D Mater.* 2014, 1, 025001.
107. Buscema, M.; Groenendijk, D.J.; Blanter, S.I.; Steele, G.A.; Van Der Zant, H.S.; Castellanos-Gomez, A. Fast and broadband photoresponse of few-layer black phosphorus field-effect transistors. *Nano Lett.* 2014, 14, 3347–3352.
108. Liu, F.; You, L.; Seyler, K.L.; Li, X.; Yu, P.; Lin, J.; Wang, X.; Zhou, J.; Wang, H.; He, H.; et al. Room-temperature ferroelectricity in CuInP2S6 ultrathin flakes. *Nat. Commun.* 2016, 7, 1–6.
109. Huang, Y.; Sutter, E.; Shi, N.N.; Zheng, J.; Yang, T.; Englund, D.; Gao, H.J.; Sutter, P. Reliable exfoliation of large-area high-quality flakes of graphene and other two-dimensional materials. *ACS Nano* 2015, 9, 10612–10620.
110. Desai, S.B.; Madhvapathy, S.R.; Amani, M.; Kiriya, D.; Hettick, M.; Tosun, M.; Zhou, Y.; Dubey, M.; Ager, J.W., III; Chrzan, D.; et al. Gold-mediated exfoliation of ultralarge optoelectronically-perfect monolayers. *Adv. Mater.* 2016, 28, 4053–4058.
111. Coleman, J.N.; Lotya, M.; O'Neill, A.; Bergin, S.D.; King, P.J.; Khan, U.; Young, K.; Gaucher, A.; De, S.; Smith, R.J.; et al. Two-dimensional nanosheets produced by liquid exfoliation of layered materials. *Science* 2011, 331, 568–571.
112. Wang, Q.H.; Kalantar-Zadeh, K.; Kis, A.; Coleman, J.N.; Strano, M.S. Electronics and optoelectronics of two-dimensional transition metal dichalcogenides. *Nat. Nanotechnol.* 2012, 7, 699–712.
113. Smith, R.J.; King, P.J.; Lotya, M.; Wirtz, C.; Khan, U.; De, S.; O'Neill, A.; Duesberg, G.S.; Grunlan, J.C.; Moriarty, G.; et al. Large-scale exfoliation of inorganic layered compounds in aqueous surfactant solutions. *Adv. Mater.* 2011, 23, 3944–3948.
114. Coleman, J.N. Liquid exfoliation of defect-free graphene. *Accounts Chem. Res.* 2013, 46, 14–22.
115. Hernandez, Y.; Nicolosi, V.; Lotya, M.; Blighe, F.M.; Sun, Z.; De, S.; McGovern, I.; Holland, B.; Byrne, M.; Gun'ko, Y.K.; et al. High-yield production of graphene by liquid-phase exfoliation of graphite. *Nat. Nanotechnol.* 2008, 3, 563–568.
116. O'Neill, A.; Khan, U.; Coleman, J.N. Preparation of high concentration dispersions of exfoliated MoS2 with increased flake size. *Chem. Mater.* 2012, 24, 2414–2421.
117. Feng, J.; Peng, L.; Wu, C.; Sun, X.; Hu, S.; Lin, C.; Dai, J.; Yang, J.; Xie, Y. Giant moisture responsiveness of VS2 ultrathin nanosheets for novel touchless positioning interface. *Adv. Mater.*

- 2012, 24, 1969–1974.
118. Zhou, K.G.; Mao, N.N.; Wang, H.X.; Peng, Y.; Zhang, H.L. A mixed-solvent strategy for efficient exfoliation of inorganic graphene analogues. *Angew. Chem.* 2011, 123, 11031–11034.
 119. Yi, M.; Shen, Z. A review on mechanical exfoliation for the scalable production of graphene. *J. Mater. Chem. A* 2015, 3, 11700–11715.
 120. Paton, K.R.; Varrla, E.; Backes, C.; Smith, R.J.; Khan, U.; O'Neill, A.; Boland, C.; Lotya, M.; Istrate, O.M.; King, P.; et al. Scalable production of large quantities of defect-free few-layer graphene by shear exfoliation in liquids. *Nat. Mater.* 2014, 13, 624–630.
 121. Liu, L.; Shen, Z.; Yi, M.; Zhang, X.; Ma, S. A green, rapid and size-controlled production of high-quality graphene sheets by hydrodynamic forces. *Rsc Adv.* 2014, 4, 36464–36470.
 122. Yu, J.; Li, J.; Zhang, W.; Chang, H. Synthesis of high quality two-dimensional materials via chemical vapor deposition. *Chem. Sci.* 2015, 6, 6705–6716.
 123. Jones, A.C.; Hitchman, M.L. Overview of chemical vapour deposition. *Chem. Vapor. Depos.* 2009, 1, 1–36.
 124. Somani, P.R.; Somani, S.P.; Umeno, M. Planer nano-graphenes from camphor by CVD. *Chem. Phys. Lett.* 2006, 430, 56–59.
 125. Pollard, A.; Nair, R.; Sabki, S.; Staddon, C.; Perdigao, L.; Hsu, C.; Garfitt, J.; Gangopadhyay, S.; Gleeson, H.; Geim, A.; et al. Formation of monolayer graphene by annealing sacrificial nickel thin films. *J. Phys. Chem. C* 2009, 113, 16565–16567.
 126. Reina, A.; Jia, X.; Ho, J.; Nezich, D.; Son, H.; Bulovic, V.; Dresselhaus, M.S.; Kong, J. Large area, few-layer graphene films on arbitrary substrates by chemical vapor deposition. *Nano Lett.* 2009, 9, 30–35.
 127. Kim, G.; Jang, A.R.; Jeong, H.Y.; Lee, Z.; Kang, D.J.; Shin, H.S. Growth of high-crystalline, single-layer hexagonal boron nitride on recyclable platinum foil. *Nano Lett.* 2013, 13, 1834–1839.
 128. Zhao, Y.; Luo, X.; Zhang, J.; Wu, J.; Bai, X.; Wang, M.; Jia, J.; Peng, H.; Liu, Z.; Quek, S.Y.; et al. Interlayer vibrational modes in few-quintuple-layer Bi₂Te₃ and Bi₂Se₃ two-dimensional crystals: Raman spectroscopy and first-principles studies. *Phys. Rev. B* 2014, 90, 245428.
 129. Zheng, W.; Xie, T.; Zhou, Y.; Chen, Y.; Jiang, W.; Zhao, S.; Wu, J.; Jing, Y.; Wu, Y.; Chen, G.; et al. Patterning two-dimensional chalcogenide crystals of Bi₂Se₃ and In₂Se₃ and efficient photodetectors. *Nat. Commun.* 2015, 6, 1–8.
 130. Mannix, A.J.; Zhou, X.F.; Kiraly, B.; Wood, J.D.; Alducin, D.; Myers, B.D.; Liu, X.; Fisher, B.L.; Santiago, U.; Guest, J.R.; et al. Synthesis of borophenes: Anisotropic, two-dimensional boron polymorphs. *Science* 2015, 350, 1513–1516.

131. Gogotsi, Y. Chemical vapour deposition: Transition metal carbides go 2D. *Nat. Mater.* 2015, 14, 1079–1080.
132. Xu, C.; Wang, L.; Liu, Z.; Chen, L.; Guo, J.; Kang, N.; Ma, X.L.; Cheng, H.M.; Ren, W. Large-area high-quality 2D ultrathin Mo₂C superconducting crystals. *Nat. Mater.* 2015, 14, 1135–1141.
133. Fleurence, A.; Friedlein, R.; Ozaki, T.; Kawai, H.; Wang, Y.; Yamada-Takamura, Y. Experimental evidence for epitaxial silicene on diboride thin films. *Phys. Rev. Lett.* 2012, 108, 245501.
134. Zhan, Y.; Liu, Z.; Najmaei, S.; Ajayan, P.M.; Lou, J. Large-area vapor-phase growth and characterization of MoS₂ atomic layers on a SiO₂ substrate. *Small* 2012, 8, 966–971.
135. Zhang, Y.; Zhang, Y.; Ji, Q.; Ju, J.; Yuan, H.; Shi, J.; Gao, T.; Ma, D.; Liu, M.; Chen, Y.; et al. Controlled growth of high-quality monolayer WS₂ layers on sapphire and imaging its grain boundary. *ACS Nano* 2013, 7, 8963–8971.
136. Wang, X.; Gong, Y.; Shi, G.; Chow, W.L.; Keyshar, K.; Ye, G.; Vajtai, R.; Lou, J.; Liu, Z.; Ringe, E.; et al. Chemical vapor deposition growth of crystalline monolayer MoSe₂. *ACS Nano* 2014, 8, 5125–5131.
137. Docherty, C.J.; Parkinson, P.; Joyce, H.J.; Chiu, M.H.; Chen, C.H.; Lee, M.Y.; Li, L.J.; Herz, L.M.; Johnston, M.B. Ultrafast transient terahertz conductivity of monolayer MoS₂ and WSe₂ grown by chemical vapor deposition. *ACS Nano* 2014, 8, 11147–11153.
138. Zhang, M.; Zhu, Y.; Wang, X.; Feng, Q.; Qiao, S.; Wen, W.; Chen, Y.; Cui, M.; Zhang, J.; Cai, C.; et al. Controlled synthesis of ZrS₂ monolayer and few layers on hexagonal boron nitride. *J. Am. Chem. Soc.* 2015, 137, 7051–7054.
139. Keyshar, K.; Gong, Y.; Ye, G.; Brunetto, G.; Zhou, W.; Cole, D.P.; Hackenberg, K.; He, Y.; Machado, L.; Kabbani, M.; et al. Chemical vapor deposition of monolayer rhenium disulfide (ReS₂). *Adv. Mater.* 2015, 27, 4640–4648.
140. Liu, L.; Park, J.; Siegel, D.A.; McCarty, K.F.; Clark, K.W.; Deng, W.; Basile, L.; Idrobo, J.C.; Li, A.P.; Gu, G. Heteroepitaxial growth of two-dimensional hexagonal boron nitride templated by graphene edges. *Science* 2014, 343, 163–167.
141. De Parga, A.V.; Calleja, F.; Borca, B.; Passeggi Jr, M.; Hinarejos, J.; Guinea, F.; Miranda, R. Periodically rippled graphene: Growth and spatially resolved electronic structure. *Phys. Rev. Lett.* 2008, 100, 056807.
142. Li, M.Y.; Shi, Y.; Cheng, C.C.; Lu, L.S.; Lin, Y.C.; Tang, H.L.; Tsai, M.L.; Chu, C.W.; Wei, K.H.; He, J.H.; et al. Epitaxial growth of a monolayer WSe₂-MoS₂ lateral p-n junction with an atomically sharp interface. *Science* 2015, 349, 524–528.
143. Yu, Y.; Hu, S.; Su, L.; Huang, L.; Liu, Y.; Jin, Z.; Puzos, A.A.; Geohegan, D.B.; Kim, K.W.; Zhang, Y.; et al. Equally efficient interlayer exciton relaxation and improved absorption in epitaxial and

- nonepitaxial MoS₂/WS₂ heterostructures. *Nano Lett.* 2015, 15, 486–491.
144. Heo, H.; Sung, J.H.; Jin, G.; Ahn, J.H.; Kim, K.; Lee, M.J.; Cha, S.; Choi, H.; Jo, M.H. Rotation-Misfit-Free Heteroepitaxial Stacking and Stitching Growth of Hexagonal Transition-Metal Dichalcogenide Monolayers by Nucleation Kinetics Controls. *Adv. Mater.* 2015, 27, 3803–3810.
145. Duesberg, G.S. Heterojunctions in 2D semiconductors: A perfect match. *Nat. Mater.* 2014, 13, 1075–1076.
146. Li, M.Y.; Chen, C.H.; Shi, Y.; Li, L.J. Heterostructures based on two-dimensional layered materials and their potential applications. *Mater. Today* 2016, 19, 322–335.
147. Shi, Z.T.; Kang, W.; Xu, J.; Sun, Y.W.; Jiang, M.; Ng, T.W.; Xue, H.T.; Denis, Y.; Zhang, W.; Lee, C.S. Hierarchical nanotubes assembled from MoS₂-carbon monolayer sandwiched superstructure nanosheets for high-performance sodium ion batteries. *Nano Energy* 2016, 22, 27–37.
148. Xie, J.; Zhang, H.; Li, S.; Wang, R.; Sun, X.; Zhou, M.; Zhou, J.; Lou, X.W.; Xie, Y. Defect-rich MoS₂ ultrathin nanosheets with additional active edge sites for enhanced electrocatalytic hydrogen evolution. *Adv. Mater.* 2013, 25, 5807–5813.
149. Xie, J.; Zhang, J.; Li, S.; Grote, F.; Zhang, X.; Zhang, H.; Wang, R.; Lei, Y.; Pan, B.; Xie, Y. Controllable disorder engineering in oxygen-incorporated MoS₂ ultrathin nanosheets for efficient hydrogen evolution. *J. Am. Chem. Soc.* 2013, 135, 17881–17888.
150. Cai, L.; He, J.; Liu, Q.; Yao, T.; Chen, L.; Yan, W.; Hu, F.; Jiang, Y.; Zhao, Y.; Hu, T.; et al. Vacancy-induced ferromagnetism of MoS₂ nanosheets. *J. Am. Chem. Soc.* 2015, 137, 2622–2627.
151. Song, H.J.; You, S.; Jia, X.H.; Yang, J. MoS₂ nanosheets decorated with magnetic Fe₃O₄ nanoparticles and their ultrafast adsorption for wastewater treatment. *Ceram. Int.* 2015, 41, 13896–13902.
152. Jeong, S.; Yoo, D.; Jang, J.t.; Kim, M.; Cheon, J. Well-defined colloidal 2-D layered transition-metal chalcogenide nanocrystals via generalized synthetic protocols. *J. Am. Chem. Soc.* 2012, 134, 18233–18236.
153. Gupta, A.; Sakthivel, T.; Seal, S. Recent development in 2D materials beyond graphene. *Prog. Mater. Sci.* 2015, 73, 44–126.
154. Wang, L.; Sun, C.; Xu, L.; Qian, Y. Convenient synthesis and applications of gram scale boron nitride nanosheets. *Catal. Sci. Technol.* 2011, 1, 1119–1123.
155. Zhang, N.; Liu, X.; Yi, R.; Shi, R.; Gao, G.; Qiu, G. Selective and controlled synthesis of single-crystalline yttrium hydroxide/oxide nanosheets and nanotubes. *J. Phys. Chem. C* 2008, 112, 17788–17795.

156. Yang, S.; Gong, Y.; Liu, Z.; Zhan, L.; Hashim, D.P.; Ma, L.; Vajtai, R.; Ajayan, P.M. Bottom-up approach toward single-crystalline VO₂-graphene ribbons as cathodes for ultrafast lithium storage. *Nano Lett.* 2013, 13, 1596–1601.
157. Shen, J.; Dong, P.; Baines, R.; Xu, X.; Zhang, Z.; Ajayan, P.M.; Ye, M. Controlled synthesis and comparison of NiCo₂S₄/graphene/2D TMD ternary nanocomposites for high-performance supercapacitors. *Chem. Commun.* 2016, 52, 9251–9254.
158. Shen, J.; Ji, J.; Dong, P.; Baines, R.; Zhang, Z.; Ajayan, P.M.; Ye, M. Novel FeNi₂S₄/TMD-based ternary composites for supercapacitor applications. *J. Mater. Chem. A* 2016, 4, 8844–8850.
159. Meng, F.; Hong, Z.; Arndt, J.; Li, M.; Zhi, M.; Yang, F.; Wu, N. Visible light photocatalytic activity of nitrogen-doped La₂Ti₂O₇ nanosheets originating from band gap narrowing. *Nano Res.* 2012, 5, 213–221.
160. Ghuman, K.K.; Hoch, L.B.; Szymanski, P.; Loh, J.Y.; Kherani, N.P.; El-Sayed, M.A.; Ozin, G.A.; Singh, C.V. Photoexcited surface frustrated Lewis pairs for heterogeneous photocatalytic CO₂ reduction. *J. Am. Chem. Soc.* 2016, 138, 1206–1214.
161. Hoch, L.B.; Szymanski, P.; Ghuman, K.K.; He, L.; Liao, K.; Qiao, Q.; Reyes, L.M.; Zhu, Y.; El-Sayed, M.A.; Singh, C.V.; et al. Carrier dynamics and the role of surface defects: Designing a photocatalyst for gas-phase CO₂ reduction. *Proc. Natl. Acad. Sci. USA* 2016, 113, E8011–E8020.

Retrieved from <https://encyclopedia.pub/entry/history/show/6569>